ACS APPLIED MATERIALS & INTERFACES

Research Article

www.acsami.org

Broad-Spectrum Antiviral Property of Polyoxometalate Localized on a Cell Surface

Juan Wang,[†] Yang Liu,[‡] Kun Xu,[†] Yanfei Qi,[†] Jun Zhong,[‡] Kai Zhang,[§] Juan Li,*[,†] Enbo Wang,[∥] Ziyu Wu,[⊥] and Zhenhui Kang*[,‡]

[†]School of Public Health, Jilin University, Changchun, Jilin 130021, China

[‡]Institute of Functional Nano & Soft Materials, Jiangsu Key Laboratory for Carbon-based Functional Materials and Devices, and Collaborative Innovation Center of Suzhou Nano Science and Technology, Soochow University, Jiangsu 215123, China

[§]Institute of High Energy Physics, Chinese Academy of Sciences, Beijing 100049, China

[∥]Faculty of Chemistry, Northeast Normal University, Changchun, Jilin 130024, China

[⊥]National Synchrotron Radiation Laboratory, University of Science and Technology of China, Hefei 230026, China

Supporting Information

ABSTRACT: $Cs_2K_4Na[SiW_9Nb_3O_{40}]$ has broad antiviral ability including anti-Influenza A, -Influenza B, -HSV-1, -HSV-2, -HIV-1, and -HBV. A series of antivirus and/or biochemical experiments and X-ray nanotomography analysis confirm that this kind of broad-spectrum antiviral property is mainly due to its localization on the cell surface.

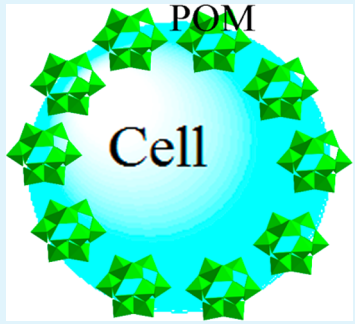

KEYWORDS: *polyoxometalate, antiviral activity, X-ray nanotomography, HepG2 cell, nanotomography technique*

INTRODUCTION

Polyoxometalates (POMs) are attractive for applications in medicine because of their generally nontoxic to normal cells, and molecular properties (such as polarity, redox potentials, surface charge distribution, shape, acidity, and structure designable) that impact the recognition and reactivity of POMs with target biological macromolecules can be altered.[1−9] Perhaps the most significant general medical property of POMs lies in their antiviral activity: diverse but specific with efficacy in vivo not simply in vitro.[9] Despite the fact that numerous POMs have been prepared and evaluated, the application of POMs to medicine and/or biosystems is still in its infancy.[9−12] Notably, the mechanism of viral inhibition of POMs is still unclear.[13,14]

The degree of cellular penetration and localization of a drug directly impacts its mechanism of viral inhibition and other biological attributes.[14] This point is a matter of direct relevance to the development of drugs that target biomolecules intracellularly including human immunodeficiency virus protease, hepatitis virus, and reverse transcriptase inhibitors.[15] Although several lines of evidence using different techniques and types of experiments[9] (Raman spectroscopy, fluorescence microscopy, electron microscopy, scanning proton microscopy, and energy-dispersive spectroscopy X-ray microanalysis) suggest that POMs could cross cell membranes, so far, definitive and direct experimental evidence to settle the controversial results for whether POMs are active at the cell surface or in the cytoplasm is scarce.

Using X-rays to construct three-dimensional (3D) tomographic images has already been well established in medicine.[16−18] Recently, the same principle was also extended to the nanoscale, bringing us startlingly accurate pictures of tiny objects, which was confirmed to be efficient for the imaging of cells.[19−21]

As reported, $K_7[SiW_9Nb_3O_{40}]$ and $(Me_3NH)_7[SiW_9Nb_3O_{40}]$ show antiviral abilities on the influenza virus (Influenza A/B), respiratory syncytical virus, murine leukemia sarcoma virus, and human immunodeficiency virus (HIV).[9−12] In our previous work, it was found that compound $Cs_2K_4Na[SiW_9Nb_3O_{40}]$ (POM93) has good anti-hepatitis B virus (HBV) properties. Herein, we report that POM93 has broad and high antivirus activities for the influenza virus (Influenza A and Influenza B), herpes simplex virus (HSV-1 and HSV-2), and HIV-1. Significantly, a series of antivirus and biochemical experiments indicated that POM93 was located on the cell surface instead of the interior of the cell. Moreover, on the basis of the X-ray nanotomography technique, we further confirmed that this kind

Received: April 11, 2014
Accepted: May 30, 2014
Published: May 30, 2014

   dx.doi.org/10.1021/am502193f | ACS Appl. Mater. Interfaces 2014, 6, 9785−9789

of broad-spectrum antiviral property of POM93 is mainly due to its localization on the cell surface.

EXPERIMENTAL SECTION

Materials. Unless stated otherwise, all reagents and chemicals were obtained from commercial sources. Sodium tungstate dihydrate (99%), potassium hydroxide (90%), hydrochloric acid (37%), niobium pentoxide (99.5%), cesium chloride (99.5%), and hydrogen peroxide (30%) were obtained from Sigma-Aldrich and used without further purification.

Synthesis of POM93. $Cs_2K_4Na[SiW_9Nb_3O_{40}]\cdot H_2O$ was prepared as described below. First, a hexaniobate solution was made by dissolving 6.5 g of $K_7H[Nb_6O_{19}]$ in 400 mL of deionized (DI) H_2O, after which 11.6 M hydrogen peroxide was added with gentle stirring. The reaction mixture was then acidified by the addition of 3 M HCl (20 mL), and 25.1 g of A-α-$Na_9H[SiW_9O_{34}]$ was mixed in until fully dissolved. The solution was diluted with DI H_2O to a final volume of 700 mL, resulting in a yellowish color. A total of 10 g of cesium chloride was added, and the solution was evaporated at room temperature. Approximately 350 mL of a yellow precipitate resulted. The entire volume of the yellow precipitate was added to 300 mL of distilled water and heated to 45 °C (>5 h) in a water bath with continual stirring. The solution was then filtered through 0.2 μm mesh and allowed to evaporate at room temperature. Within only a few minutes, yellow-colored crystals of $Cs_2K_4Na[SiW_9Nb_3O_{40}]\cdot H_2O$ developed (the X-ray diffraction pattern of POM93 is shown in Figure S1 in the Supporting Information, SI). Elemental analysis was carried out on the crystalline $Cs_2K_4Na[SiW_9Nb_3O_{40}]\cdot H_2O$ ($H_2Cs_2K_4NaNb_3O_{41}SiW_9$). Weight percents were as follows (expected/actual): Cs, 8.67/8.97; K, 5.09/4.93; Nb, 9.09/9.19; W, 54.02/54.15. IR spectral values (see Figure S2 in the SI) measured by the KBr pellet method (cm^{-1}) were 3429, 2357, 1623, 990, 958, 868, 789, 673, 595, 534, and 474.

Antivirus Activity Assay of POM93. The antiviral activities were assayed by the MTT method. MDCK cells (for the influenza virus), Vero cells (for HSV), and MT-4 cells (for HIV-1) were seeded in a 96-well plate at a seeding density of 2×10^5 viable cells/mL and incubated for 24 h at 37 °C, followed by the addition of 0.1 mL of Influenza A/Influenza B/HSV-1/HSV-2/HIV-1 virus stock and various doses of POM93 (0.1 mL) to each well. In addition, 0.1 mL of the medium was added as the negative control group. Then the plates were incubated for 2 days at 37 °C in a humidified atmosphere containing 5% CO_2 until maximum cytopathic effects (CPEs) were observed in the negative control (untreated cells). The CPE was observed by using MTT colorimetric assay. Briefly, 20 μL of the MTT stock solution prepared in Dulbecco's modified eagle medium was added to each well, and the plates were incubated for a further 4 h at 37 °C. After incubation, the residual MTT solution in each well was carefully removed, without disturbing the formazan crystals. The formazan crystals were dissolved by adding 150 μL of dimethyl sulfoxide (DMSO) to each well, and the plates were gently shaken for another 5 min. The quantity of MTT reduction was measured immediately by detecting the absorbance at 570 nm. The rates of protection were calculated as $(A - B)/(C - B) \times 100\%$, where A, B, and C mean the absorbance values from wells containing POM93 and virus A, virus B, and cell (C) only, respectively.

Cytotoxicity Analysis. The cytotoxicity of POM93 was determined using direct MTT assay. Briefly, MDCK, Vero, and HepG2 cells were seeded on 96-well plates at a seeding density of 5.0×10^4 cells/mL and incubated for 24 h at 37 °C, followed by the addition of various concentrations of POM93 and ADV to each well. In addition, an equal volume of the medium was added as the negative control group. After 48 h of incubation as required, 20 μL of an MTT solution [5 mg/mL in 0.01 M phosphate buffered saline (PBS)] was added to each well. Cells were incubated for an additional 4 h at 37 °C, and then 0.15 mL of DMSO was added to the mixture. The cytotoxic activity was evaluated by the reduction of MTT observed in mitochondria at 48 h after the initial treatment. The amount of MTT reduction was measured by reading the absorbance using a plate reader (Bio-Rad Co.) at a wavelength of 570 nm. CC_{50} was defined as the concentration of the compound that reduced the viable cell number by 50% and calculated using the Bliss method.

RESULTS AND DISCUSSION

In our experiments, compound POM93 was synthesized by a mild wet chemical approach developed by our research group, and the synthetic details are shown in the Experimental Section. The antivirus activities and cytotoxicities of POM93 were estimated by 3-(4,5-dimethylthiazol-2-yl)-2,5-diphenyltetrazolium bromide (MTT) assay. Details of the antiviral activity and cytotoxicity are shown in Table 1. Data were expressed as mean ± SD (standard deviation). From it, we can see that POM93 possesses high antivirus activities with low EC_{50} (the 50% virus-inhibitory effective concentration) on Influenza A, Influenza B, HSV-1, HSV-2, and HIV-1 and low cytotoxicity with high CC_{50} (the 50% cell-inhibitory concentration) on MDCK, Vero, and MT-4 cells.

Table 1. Antiviral Activity and Cytotoxicity of POM93 in Vitro

virus	cell line	EC_{50} (μg/mL)	CC_{50} (μg/mL)
Influenza A[a]	MDCK	7.4 ± 1.1	426.2 ± 8.7
Influenza B	MDCK	11.2 ± 3.1	475.2 ± 6.9
HSV-1	Vero	2.5 ± 1.3	1060.5 ± 9.3
HSV-2	Vero	7.3 ± 1.6	1358.5 ± 8.5
HIV-1	MT-4	3.2 ± 0.8	325.7 ± 5.4
HBV[b]	HepG2	11.4 ± 0.6	1784.0 ± 3.1

[a]Influenza A virus here only including H1N1. [b]Data from our previous work in ref 12.

It was known that the sequential stages of HSV entry into the host cell are analogous to those of other enveloped viruses. Typically, the virus particle is covered by an envelope, which, when bound to specific receptors on the cell surface, will fuse with the cell membrane and create an opening, or pore, through which the virus enters the host cell. As reported, the pretreatment of Vero cells with $K_7[PTi_2W_{10}O_{40}]\cdot 6H_2O$ (PM-19) prior to HSV-2 infection enhanced the antiviral potency of PM-19 (called the "memory effect"), in which PM-19 mainly inhibits HSV-2 infection at the penetration stage.[22,23] In light of this, in our biochemical experiments (the experimental design is shown in Figure 1, similar to ref 23), Vero cell monolayers were washed with PBS and then infected with HSV-2 at 100 PFU per well in the presence of POM93 for various periods. After attachment of the virus to cells for 60 min at 4 °C, the cells were washed with PBS and then overlaid with an agar overlay

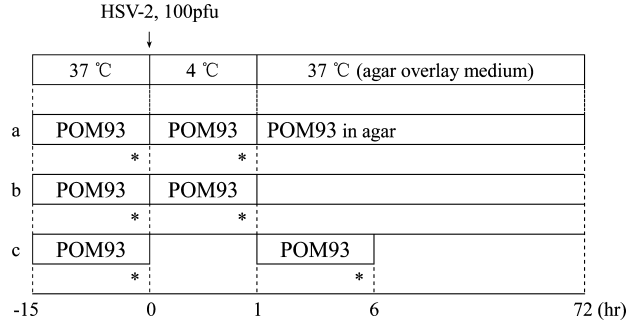

Figure 1. Experimental design for investigation of the pretreatment effects of POM93.

medium. The results of plaque assay were expressed as plaque numbers per well. It was found that POM93-treated Vero cells had an altered response to HSV-2 infection, and the plaque inhibition effect was determined with cells pretreated or nontreated with POM93. Pretreatment with POM93 for 15 h prior to infection did not influence the plaque formation after HSV-2 infection (Table 2, group a; POM93, 0 μg/mL). In addition, the pretreated Vero cells as well as nontreated cells (data not shown) grew. The readdition of POM93 at concentrations above 20 μg/mL from 0 to 72 h after infection caused complete inhibition of plaque formation. However, no effect of the pretreatment with POM93 was found (Table 2, group a). In contrast, inhibition of viral attachment and penetration by POM93 was enhanced in cells pretreated with POM93. As shown in Table 2, with pretreatment by POM93, there are obvious antivirus effects of POM93 on the first (0−1 h, group b) and second (1−6 h, group c) stage of HSV-2 infection. In order to further confirm the pretreatment effects of POM93, in a further control experiment, acyclovir (ACV; based on selective inhibition of the replication of herpes viruses and because a triphosphate acyclovir inhibits the DNA polymerase and thus the formation of viral DNA)[24,25] pretreated and nontreated Vero cells were infected with HSV-2 at 100 PFU per well and then retreated with ACV at 2 μg/mL to determine the effect on replication of HSV-2. The results are expressed as the number of plaques (see Table S1 in the SI). From it, we can see that there is no obvious antivirus effect of ACV on the first (0−1 h) and second (1−6 h) stages of HSV-2 infection. These pretreatment effects of POM93 were similar to the "memory effect" of PM-19,[23] which inhibited HSV-2 infection at the adsorption and/or penetration stage, and inferred that almost all POM93 should locate on the cell surface instead of the interior of the cell.[23]

Table 2. HSV-2 Replication of Vero Cells with Exposure to Various Concentrations of POM93

		no. of plaques	
group	dose (μg/mL)	N*	P**
a	0	90	92
	5	88	90
	20	32	27
	80	9	8
b	20	65	39
	80	41	25
c	20	39	16
	80	12	7

Treated with POM93: group a, 0−72 h; group b, 0−1 h; group c, 1−6 h. N* = not pretreated with POM93; P** = pretreated with POM93.

It should be further pointed out that, as shown in Table 1, POM93 has a broad-spectrum antiviral property. Here, the question is whether this kind of broad-spectrum antiviral property is attributed to its location on the cell surface. All of the above antiviral experimental results suggested that POM93 should be located on the cell surface; however, there is still a lack of direct evidence to confirm it. Nanotomography, as a powerful and unique technique, with pixel sizes of the cross sections in the nanometer range, uses X-rays to create cross sections from a 3D object that later can be used to recreate a virtual model without destroction of the original model.[19−21] Thus, in the following experiments, X-ray nanotomography tests were carried out.

The following nanotomography experiment was carried out using full-field X-ray microscopy at the 4W1A beamline of the Beijing Synchrotron Radiation Facility. In the experiment, after the incident X-ray was focused onto the sample by using a condenser consisting of an elliptically shaped capillary tube, the X-ray image of the sample was then magnified by the objective stacked zone plates with a 45 nm outermost zone width operated at 8 keV. Hereafter, the magnified image was converted into a visual one on the YAG-Ce scintillator screen. This visual image is further enlarged 20 times with a microscope objective lens and captured by a 1024 × 1024 pixel CCD camera. The resolution was tested using the electroplated gold spoke patterns, which shows that the resolution can reach 50 nm with the field of view of 15 × 15 μm^2 and a pixel size of 15 × 15 nm.

In X-ray nanotomography tests, the HepG2 cells (the sample process with graded dehydration has preserved the overall morphology of the cells relatively well) were spotted on a mylar membrane of 20 μm thickness and dried in air. We used tomography to reveal the distribution of POM93 in a HepG2 cell. Because the contrast of pure cell is very low under hard X-ray, POM93 will show high contrast in the obtained image, and their distribution thus can be identified. The experiments were carried out at 8 keV by placing the phase ring in the back focal plane of the objective zone plate, which can provide Zernike phase contrast and was suitable for investigating light materials. The tomography images of HepG2 were collected at 0.25° intervals from −60° to +60° and saved in the computer with an exposure time of 30 s per image; the total scanning time was about 4 h. After tomography data acquisition, all of the projective images needed to be corrected to a common axis of rotation using gold particles with 0.8−1.5 μm diameter as reference markers. Finally, using a parallel-beam filtered-back-projection algorithm, the 3D and slice images of a HepG2 cell were reconstructed and are shown in Figure 2. From the 3D reconstruction, a series of cross-sectional slices can be generated through the cell from any orientation without the need for actual sectioning. Two representative one-pixel-thick (about 15 nm) reconstructed slices, in which the gray value of each pixel corresponds to the density and phase information on the sample, are shown in Figure 2a,b. Figure 2a shows the *XZ* plane slice, and only a circle for the cell wall can be identified

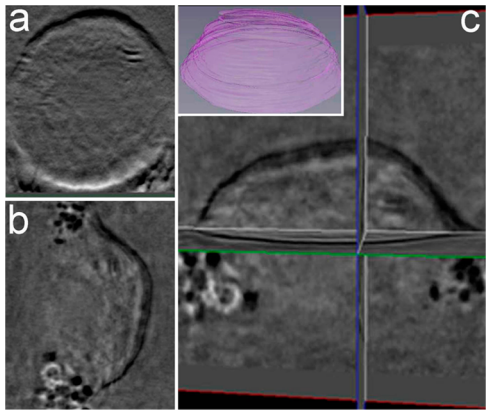

Figure 2. X-ray nanotomography imaging results of a HepG2 cell treated with POM93 (100 μg/mL): (a) *XZ* plane; (b) *YZ* plane; (c) green, red, and blue for the *XZ*, *YZ*, and *XY* planes, respectively. The inset shows a 3D image of the HepG2 cell.

with high contrast, suggesting that POM93 was deposited on the cell wall. Figure 2b shows the *YZ* plane slice, and the cell wall is also clear, without obvious signals inside indicating nanoparticle distribution on the cell wall. The shape of the HepG2 cell looks like a bowl in Figure 2b because the cell collapses on the membrane. The open side of the bowl is the membrane, and the clusters of dark objects around the cell are gold particles used as markers. Figure 2c shows the magnified image of the cell on the *YZ* plane, and the green line indicates the *XZ* plane while the blue line indicates the *XY* plane. The inset shows a 3D image of the cell. It is clear that the whole cell looks like a bowl with the high-contrast cell wall and nothing inside. A series of slices throughout the whole cell can be played back as videos (videos 1 and 2 in the SI) showing all structures of the cell, and the data confirm that our POM93 mainly deposits on the cell wall.

Here we also want to further point out that POMs are a class of metal oxide cluster anion compounds that exhibit antiviral activity properties. Many studies have found evidence that POMs can inhibit replication of a broad variety of both RNA and DNA viruses in vitro and in vivo.[9,26−30] In this study, the X-ray nanotomography technique confirmed that this kind of broad-spectrum antiviral property of POM93 is mainly due to its localization on the cell surface. The nonspecific masking of the cell by POM93 prevents virus entry into the cell, leading to viral inhibition. The antiviral activity of POM93 may be as an inhibitor of the binding and fusion process. However, POMs may break down into constituent metal-containing components, and this kind of breakdown and/or accumulation under biological conditions, particularly in the kidneys and in the liver, accounts for the lack of interest in further study.[31] Accordingly, toxic affects account for the lack of interest in the further development of these potential medicinal candidate drugs. Anyway, based on the structural feature, broad antivirus activities, and clear action of localization on the cell surface, POMs should be regarded as a new type of antiviral agent.

CONCLUSION

In summary, we reported that compound $Cs_2K_4Na[SiW_9Nb_3O_{40}]$ (POM93) has broad and high antivirus activities of Influenza A/Influenza B, HSV, HIV, HBV, and HCV. A series of antivirus and biochemical experiments indicated that POM93 was located on the cell surface instead of the interior of the cell. Further, the X-ray nanotomography experiments confirmed that this kind of broad-spectrum antiviral property of POM93 is mainly due to its localization on the cell surface. Our results suggest that POM93 with the character of location on the cell surface may be a new type of antiviral agent. Moreover, the present work also is an example for the deep study in inorganic drugs or the biological effect of inorganic nanomaterials based on the X-ray nanotomography technique.

ASSOCIATED CONTENT

Supporting Information

Plaque assay of POM93 pretreatment on HSV-2, the effect of ACV pretreatment on HSV-2 replication, and videos 1 and 2. This material is available free of charge via the Internet at http://pubs.acs.org.

AUTHOR INFORMATION

Corresponding Authors

*E-mail: li_juan@jlu.edu.cn..

*E-mail: zhkang@suda.edu.cn.

Notes

The authors declare no competing financial interest.

ACKNOWLEDGMENTS

We are thankful for the support of the National Basic Research Program of China (973 Program; Grants 2012CB825800 and 2013CB932702), National Natural Science Foundation of China (Grant 51132006), Specialized Research Fund for the Doctoral Program of Higher Education (Grant 20123201110018), a project funded by the Priority Academic Program Development of Jiangsu Higher Education Institutions, and the Talents Ph.D. Project of Bethune College of Medicine in Jilin University. Here, we also celebrate over 50 years of contributions of Prof. Enbo Wang to education at Northeast Normal University.

REFERENCES

(1) Zhang, J.; Song, Y. F.; Cronin, L.; Liu, T. B. Self-Assembly of Organic−Inorganic Hybrid Amphiphilic Surfactants with Large Polyoxometalates as Polar Head Groups. *J. Am. Chem. Soc.* **2008**, *130*, 14408−14409.

(2) Fernandez, J. A.; Lopez, X.; Bo, C.; de Graaf, C.; Baerends, E. J.; Poblet, J. M. Polyoxometalates with Internal Cavities: Redox Activity, Basicity, and Cation Encapsulation in $[X^{n+}P_5W_{30}O_{110}]^{(15-n)-}$ Preyssler Complexes, with X = Na^+, Ca^{2+}, Y^{3+}, La^{3+}, Ce^{3+}, and Th^{4+}. *J. Am. Chem. Soc.* **2007**, *129*, 12244−12253.

(3) Schmitz, K. S. Macroion Clustering in Solutions and Suspensions: The Roles of Microions and Solvent. *J. Phys. Chem. B* **2009**, *113*, 2624−2638.

(4) Kong, X. J.; Long, L. S.; Zheng, Z. P.; Huang, R. B.; Zheng, L. S. Keeping the Ball Rolling: Fullerene-like Molecular Clusters. *Acc. Chem. Res.* **2010**, *43*, 201−209.

(5) Lunkenbein, T.; Kamperman, M.; Li, Z. H.; Bojer, C.; Drechsler, M.; Forster, S.; Wiesner, U.; Muller, A. H. E.; Breu, J. Direct Synthesis of Inverse Hexagonally Ordered Diblock Copolymer/Polyoxometalate Nanocomposite Films. *J. Am. Chem. Soc.* **2012**, *134*, 12685−12692.

(6) Long, D. L.; Burkholder, E.; Cronin, L. Polyoxometalate Clusters, Nanostructures and Materials: From Self-Assembly to Designer Materials and Devices. *Chem. Soc. Rev.* **2007**, *36*, 105−121.

(7) Pope, M. T.; Müller, A. Polyoxometalate Chemistry: An Old Field with New Dimensions in Several Disciplines. *Angew. Chem., Int. Ed. Engl.* **1991**, *30*, 34−48.

(8) Pope, M. T.; Müller, A. *Polyoxometalates: From Platonic Solids to Antiretroviral Activity*; Kluwer: Dordrecht, The Netherlands, 1994.

(9) Rhule, J. T.; Hill, C. L.; Judd, D. A.; Schinazi, R. F. Polyoxometalates in Medicine. *Chem. Rev.* **1998**, *98*, 327−358.

(10) Ni, L.; Greenspan, P.; Gutman, R.; Kelloes, C.; Farmer, M. A.; Boudinot, F. D. Cellular Localization of Antiviral Polyoxometalates in J774 Macrophages. *Antiviral Res.* **1996**, *32*, 141−148.

(11) Berry, J. P.; Galle, P. Subcellular Localization of HPA-23 in Different Rat Organs: Electron Microprobe Study. *Exp. Mol. Pathol.* **1990**, *53*, 255−264.

(12) Zhang, H.; Qi, Y. F.; Ding, Y. H.; Wang, J.; Li, Q. M.; Zhang, J. Z.; Jiang, Y. F.; Chi, X. M.; Li, J.; Niu, J. Q. Synthesis, Characterization and Biological Activity of a Niobium-Substituted Heteropolytungstate on Hepatitis B Virus. *Bioorg. Med. Chem. Lett.* **2012**, *22*, 1664−1669.

(13) Shigeta, S.; Mori, S.; Kodama, E.; Kodama, J.; Takahashi, K.; Yamase, T. Broad Spectrum Anti-RNA Virus Activities of Titanium and Vanadium Substituted Polyoxotungstates. *Antiviral Res.* **2003**, *58*, 265−271.

(14) Yamase, T. Anti-Tumor, -Viral, and -Bacterial Activities of Polyoxometalates for Realizing an Inorganic Drug. *J. Mater. Chem.* **2005**, *15*, 4773−4782.

(15) Judd, D. A.; Nettles, J. H.; Nevins, N.; Snyder, J. P.; Liotta, D. C.; Tang, J.; Ermolieff, J.; Schinazi, R. F.; Hill, C. L. Polyoxometalate HIV-1 Protease Inhibitors. A New Mode of Protease Iinhibition. *J. Am. Chem. Soc.* **2001**, *123*, 886−897.

(16) Attwood, D. Microscopy: Nanotomography Comes of Age. *Nature* **2006**, *442*, 642−643.
(17) Withers, P. J. X-Ray Nanotomography. *Mater. Today* **2007**, *10*, 26−34.
(18) Larabell, C. A.; Le Gros, M. A. X-Ray Tomography Generates 3-D Reconstructions of the Yeast, Saccharomyces cerevisiae, at 60-nm Resolution. *Mol. Biol. Cell* **2004**, *15*, 957−962.
(19) Jade, B. A.; Aviva, L.; Peter, A. L. Studies on the Biotransformations and Biodistributions of Metal-Containing Drugs Using X-Ray Absorption Spectroscopy. *Curr. Top. Med. Chem.* **2011**, *11*, 553−571.
(20) Uchida, M.; McDermott, G.; Wetzler, M.; Le Gros, M. A.; Myllys, M.; Knoechel, C.; Barron, A. E.; Larabell, C. A. Soft X-ray Tomography of Phenotypic Switching and the Cellular Response to Antifungal Peptoids in Candida albicans. *Proc. Natl. Acad. Sci. U.S.A.* **2009**, *106*, 19375−19380.
(21) Schneider, G.; Guttmann, P.; Heim, S.; Rehbein, S.; Mueller, F.; Nagashima, K.; Heymann, J. B.; Muller, W. G.; McNally, J. G. Three-Dimensional Cellular Ultrastructure Resolved by X-Ray Microscopy. *Nat. Methods* **2010**, *7*, 985−987.
(22) Dan, K.; Miyashita, K.; Seto, Y.; Fujita, H.; Yamase, T. Mechanism of the Protective Effect of Heteropolyoxotungstate against Herpes Simplex Virus Type 2. *Pharmacology* **2003**, *67*, 83−89.
(23) Dan, K.; Miyashita, K.; Seto, Y.; Fujita, H.; Yamase, T. The Memory Effect of Heteropolyoxotungstate (PM-19) Pretreatment on Infection by Herpes Simplex Virus at the Penetration Stage. *Pharmacol. Res.* **2002**, *46*, 357−362.
(24) Elion, G. B. The Biochemistry and Mechanism of Action of Acyclovir. *J. Antimicrob. Chemother.* **1983**, *12*, 9−17.
(25) Pesola, J. M.; Coen, D. M. In Vivo Fitness and Virulence of a Drug-Resistant Herpes Simplex Virus 1 Mutant. *J. Gen. Virol.* **2007**, *88*, 1410−1414.
(26) Yang, Y.; Li, W.; Liu, G.; Zhang, X.; Chen, J.; Wu, W.; Guan, Y.; Xiong, Y.; Tian, Y.; Wu, Z. 3D Visualization of Subcellular Structures of Schizosaccharomyces Pombe by Hard X-Ray Tomography. *J. Microsc.* **2010**, *240*, 14−20.
(27) Kak, A. C.; Slaney, M. *Principles of Computerized Tomographic Imaging*; IEEE Press: New York, 1988.
(28) Weeks, M. S.; Hill, C. L.; Schinazi, R. F. Synthesis, Characterization and Anti-Human Immunodeficiency Virus Activity of Water-Soluble Salts of Polyoxotungstate Anions with Covalently Attached Organic Groups. *J. Med. Chem.* **1992**, *35*, 1216−1221.
(29) Ikeda, S.; Neyts, J.; Yamamoto, N.; Murrer, B.; Theobald, B.; Bossard, G.; Henson, G.; Abrams, M.; Picker, D.; De Clercq, E. *In Vitro* Activity of a novel series of Polyoxosilicotungstates against Human Myxo-, Herpes-, and Retroviruses. *Antiviral Chem. Chemother.* **1993**, *4*, 253−262.
(30) Ikeda, S.; Nishiya, S.; Yamamoto, A.; Yamase, T.; Nishimura, C.; De Clercq, E. Activity of the Keggin Polyoxotungstate PM-19 against Herpes Simplex Virus Type 2 Inffection in Immunosuppressed Mice: Role of Peritoneal Macrophage Activation. *J. Med. Virol.* **1993**, *41*, 191−195.
(31) Ni, L.; Boudinot, F. D.; Boudinot, S. G.; Henson, G. W.; Bossard, G. E.; Martellucci, S. A.; Ash, P. W.; Fricker, S. P.; Darkes, M. C.; Theobald, B. R. Pharmacokinetics of Antiviral Polyoxometalates in Rats. *Antimicrob. Agents Chemother.* **1994**, *38*, 504−510.